Journal of MATERIALS RESEARCH

Invited Paper
DOI:10.1557/s43578-021-00373-5

Low-temperature annealing of 2D $Ti_3C_2T_x$ MXene films using electron wind force in ambient conditions

Md. Abu Jafar Rasel[1], Brian Wyatt[2], Maxwell Wetherington[3], Babak Anasori[2,a)], Aman Haque[1,a)]

[1] Department of Mechanical Engineering, Penn State University, University Park, PA 16802, USA
[2] Department of Mechanical and Energy Engineering, and Integrated Nanosystems Development Institute, Indiana University–Purdue University Indianapolis, Indianapolis, IN 46202, USA
[3] Materials Characterization Laboratory, Penn State University, University Park, PA 16802, USA
[a)] Address all correspondence to these authors. e-mails: banasori@iupui.edu; mah37@psu.edu

Received: 9 May 2021; accepted: 31 August 2021

Two-dimensional transition metal carbides and nitrides, known as MXenes, are layered materials with unique functionalities which make them suitable for applications such as energy storage devices, supercapacitors, electromagnetic interference shielding, and wireless communications. Since they are wet-processed, MXenes need annealing to improve their electrical conductivity. The extent of annealing highly depends on temperature; however, higher temperatures can also impact the resulting phases and structure. In this study, we present a non-thermal annealing process utilizing an electron wind force (EWF) method in ambient conditions. This process is demonstrated on freestanding $Ti_3C_2T_x$ films, where we show up to 70% decrease in resistivity at temperatures below 120 °C compared to conventional thermal annealing methods. MXene structures before and after annealing are analyzed using Raman spectroscopy and ex situ and in situ X-ray diffraction. Surface terminations and intra-flake defects modification in $Ti_3C_2T_x$ layers after EWF annealing impart better electrical conductivity to MXene film than the non-annealed films.

Introduction

2D layered transition metal carbides or nitrides, commonly known as MXenes, are emerging materials which have attracted extensive scientific research interest for their unique atomic-scale layered structure [1, 2], high electrical conductivity (20,000 S cm^{-1}) [3], impressive thermal stability [4], and scalable processing methods [5, 6]. Their chemical and structural variability [7–10], surface chemistry [11], interlayer spacing tunability [12], and attractive electrical properties [13, 14] make them strong candidates for a diverse range of applications such as lithium ion batteries [15], electrode materials [16], supercapacitors [14–20], electromagnetic interference (EMI) shielding [21, 22], and water purification [23, 24]. MXenes are mostly derived from their MAX phase precursor (e.g., Ti_3AlC_2, Ti_2AlC, and Ta_4AlC_3). A MAX phase is denoted by the chemical formula $M_{n+1}AX_n$, where M is an early transition metal, A is an element of the A group mostly of groups 13 or 14 of the periodic table (in particular, Al, Si, and Ga) and X stands for carbon and/or nitrogen. MAX is a layered material, where $n+1$ layers of M are interleaved by n layers of X (where X are in the octahedral interstices of the hexagonal M structure) with A groups bonded to the outside of the $M_{n+1}X_n$ structure [25]. MXene is derived from MAX through exfoliation by selective etching of the A element from the parent MAX phases with hydrofluoric acid-containing wet chemical solutions [20, 26, 27] or molten salts [28] as selective etchants. MXenes are similarly chemically denoted to MAX as $M_{n+1}X_nT_x$, where T_x stands for surface groups, commonly –OH, = O, –F, and –Cl [9] which are gained due to the etching method after removing the A element [29]. Surface functional groups have shown to play an important role in controlling the electrochemical [30, 31] and electronic [31] properties of MXene. $Ti_3C_2T_x$ is the most commonly studied MXene, appearing over 70% of MXene-related publications to date [32].

The combination of the effects of MXenes M-X interior and surface groups are shown to majorly impact the structure and properties of MXene flakes in both single flake and film forms

[33] and post-treatment of MXenes by thermal annealing can be used to illustrate the effects of these compositions experimentally. Several studies have described thermal annealing and calcination as an effective way to alter MXene's behavior by removing intercalants and surface terminations [4, 34–37]. Thermal annealing of films of MXene flakes has been performed in the literature in the 150–1500 °C range. In water and oxygen-containing environments, MXenes have been reported to undergo structural oxidation [38, 39] and it increases in severity as the ambient temperature is increased [38]. This structural oxidation has shown detrimental effects on the metallic electrical conductivity of the MXene [38]. However, the oxidation of MXene films during thermal annealing can be inhibited by annealing in a vacuum or inert environment [4, 34, 40]. The annealing of $Ti_3C_2T_x$ MXene flakes, while not in an oxidative environment, can be separated into three distinct regions. First, the intercalated water is removed as the temperature increases from room temperature (RT) to 200 °C [41]. The removal of intercalated water between MXene flakes in $Ti_3C_2T_x$ films has shown a decrease in sheet resistance of 18% at 200 °C [34]. Thermal properties are also shown to improve due to interlayer distance reduction from 13.62 to 11.74 Å at about at 475 °C [42]. Second, the surface groups of $Ti_3C_2T_x$ are removed with –OH as the first to be removed at 300–500 °C followed by –F at 750 °C with complete surface group loss at temperatures beyond 800 °C [34]. De-functionalization of –F content of T_x on $Ti_3C_2T_x$, which occurs from 400 to 775 °C under vacuum, illustrates a reduction of resistance by ~ 75% [34]. This reduction in resistance is associated with an increase in intra-flake carrier concentration in defunctionalized $Ti_3C_2T_x$ [34]. Third, structural phase transformations of $Ti_3C_2T_x$ to mixed present phases of $Ti_3C_2T_x$, cubic TiC_y, and cubic Ti_2C and ordered carbon vacancy superstructure of TiC_y, take place from 700 to 1500 °C [4]. In general, thermal annealing has improved the electrical conductivity in MXene films, but the required temperatures (~ 100–500 °C) make MXenes films prone to oxidation in ambient oxygen-containing conditions [43].

In this study, we present a novel, non-thermal process to achieve similar increase in electrical conductivity to those of thermal annealing of $Ti_3C_2T_x$ MXene films. We explore annealing with the electron wind force in $Ti_3C_2T_x$ in ambient conditions to improve electrical conductivity. In a conducting material, electrons are scattered by both lattice atoms and defects and interfaces. Lattice scattering causes Joule heating, which can lead to thermal runaway if not controlled. Defect scattering involves a momentum change of the impinging electrons, giving rise to a mechanical force, known as the electron wind force (EWF) [44]. Since the force is highly localized at the defects, we hypothesize that it can impart very high mobility to the defects, even though the global average of the EWF is small. Therefore, EWF can be effectively used to minimize the defect density and consequently to improve electrical conductivity as long as the dominating Joule heating effect can be avoided. In the absence of Joule heating, the defect scattering rate will dominate over lattice scattering and the EWF effects become significant. The scattering intensity can be controlled with high current density to provide a unique pathway to decrease defects concentration, grain boundary density [44–46], and improve electron mobility in layered MXene film and, thus, lower the resistivity. For example, the surface terminations can be seen as atomic defects, which can be dislodged at sufficiently high current density. Similarly, EWF can mobilize the intercalated water molecules to reduce the interlayer distance. Analytical tools such as X-ray diffraction (XRD) or Raman spectroscopy tools can be used to confirm these events to explain the decrease of electrical resistivity in EWF-annealed specimens.

In this study, we achieve EWF annealing through minimization of Joule heating by attaching the $Ti_3C_2T_x$ MXene film on a large heat sink (thick slab of aluminum nitride). We demonstrate the proposed approach on $Ti_3C_2T_x$ films at lower than 120 °C temperature with significant (72%) decrease in resistivity after applying only 377.27 Amp/mm^2 current density. In addition, we show that the resistivity change was permanent and did not increase back over time after the current was removed. In order to analyze MXenes' structure after EWF annealing, we used Raman spectroscopy to show a decrease of functional groups on MXenes' surface and no formation of disordered carbon state as seen in high-temperature annealed samples [47]. We also utilize ex situ and in situ X-ray diffraction (XRD) to display that there is no significant change in MXene inter-flake spacing to illustrate the primary role of EWF in decreasing of the resistivity. As a result, we believe that EWF processes on MXene films can provide a useful method to increase the conductivity of MXene films without the need for controlled environments and detrimental side effects of thermal annealing.

Materials and methods

$Ti_3C_2T_x$ synthesis and EWF annealing

$Ti_3C_2T_x$ is derived from its precursor MAX phase Ti_3AlC_2 via selective acid etching of Ti_3AlC_2 in a mix of hydrofluoric (HF) and hydrochloric (HCl) acid solution. In brief, Ti_3AlC_2 is synthesized through pressure less sintering of a powder mixture of TiC, Al, and Ti in a molar ratio of 2:1:1. The powder is mixed through ball milling in a polycarbonate container with yttria-stabilized zirconia balls with a ball-to-powder mass ratio of 2:1 for 18 h in a Shimpo PTA-02 jar. After mixing, the powder is reactively sintered in a Carbolite Gero furnace at 1400 °C for 2 h under Ar gas flow. After sintering, the MAX block is then turned to powder through drilling with a TiN coated drill bit. To synthesize $Ti_3C_2T_x$ MXene, 4 g of Ti_3AlC_2 powder is selectively etched through immersion in an acid mixture

comprised of 12 mL HF (50% stock, MilliporeSigma), 72 mL HCl (37% stock, MilliporeSigma), and 36 mL de-ionized water in a high-density polyethylene (HDPE) container stirred at 400 RPM at 35 °C for 24 h in an oil bath. After selective etching, the solution is then repeatedly washed with de-ionized water (300 mL de-ionized water per gram of Ti_3AlC_2) until neutral through addition of water followed by centrifugation at 3320 RCF until the pH is > 6. After washing to neutral, the $Ti_3C_2T_x$ powder is then delaminated to single-flake $Ti_3C_2T_x$ flakes through addition of $Ti_3C_2T_x$ powder to 4 g of anhydrous LiCl (Fisher Scientific) in 200 mL de-ionized water in a high-density polyethylene (HDPE) container which is stirred at 1000 RPM at 60 °C for 1 h under argon flow in an oil bath. After delamination, the powder is washed (200 mL de-ionized water per gram of Ti_3AlC_2) to remove any remaining salts to yield the final aqueous $Ti_3C_2T_x$ solution (~ 2 mg/mL). To make the $Ti_3C_2T_x$ MXene films, 10 mL of this solution and 10 mL of de-ionized water is filtered over a 0.8 µm pore size membrane using vacuum filtration. After filtration, these films are then peeled off of the filter paper and dried in vacuum to remove any excess water. To anneal the MXene films via EWF, the specimen is mounted on an aluminum nitride slab that has very high thermal conductivity (> 170 W/mK), high electrical insulation capacity (> 1.10^{12} Ωcm) and low thermal expansion 4 to 6 × 10^{-6} K^{-1} between 20 and 1000 °C (Stanford Advanced Materials). The slab itself is mounted on a custom built cold plate. Electrical connections are made with silver paste. Resistance is measured from I-V curve and converted to resistivity by multiplying with constant cross-sectional area and dividing by length. The resistivity measurement is done at low temperatures, which preclude any errors due to thermal expansion or thermal coefficient of resistivity.

Raman spectroscopy

We used a Horiba LabRam HR Evolution instrument with 50 × long working distance (numerical aperture = 0.5) objective with Duoscan spot size diameter of 20 µm (averaged analysis area via galvo-mirror control of the laser position) to help reduce effective power density of the laser and increase statistical significance of measured Raman response from each specimen. Initial characterization was performed to confirm sample composition and the safe power limit. Spectral response obtained with the 785 nm laser, 300 gr/mm grating and a confocal hole of 200 µm was very similar to that reported [48], with the exception of two peaks at 509 cm^{-1} and 1245 cm^{-1}). Laser power was maintained at about 1.7 mW (3.2%) to avoid irradiation damage. We observed traces of TiO_2 (Anatase) at power as low as 2 mW. Lorentzian peak fitting was performed in the Origin software.

X-ray diffraction

$Ti_3C_2T_x$ MXene control and EWF-annealed films were prepared for XRD scanning by cutting the films into approximately 1 cm × 1 cm squares which were subsequently placed on double-sided amorphous carbon tape mounted on an amorphous glass slide. The XRD scans were conducted using a Bruker D8 Discover X-ray diffractometer using a Cu Kα X-ray emitter ($\lambda = 1.5418$ Å) paired with a Vantec-500 XRD^2 detector. The sample height was considered focused when two alignment dual laser beams made one single laser beam point. XRD^2 scans were conducted from 5° to 75° 2θ using a step size of 5° 2θ with a timestep of 60 s (total 15 min scan). The spectra were then gathered by integrating the full 2D diffraction pattern in Bruker's EVA software with a gamma integration scheme. $Ti_3C_2T_x$'s c-lattice parameter was then calculated using the (002) reflection of $Ti_3C_2T_x$ through Bragg's Law. In situ XRD techniques were carried out with similar scan times to that of ex situ scans, while the annealing was carried out using an Anton-Parr DHS 1100 four circle goniometer hot stage by affixing the $Ti_3C_2T_x$ films to an AlN stage with stainless steel clips and ramping from room temperature (carried out at 40 °C as the ambient atmosphere was roughly 28–32 °C) up to each set temperature (600, 700, 800, 900 °C) sequentially at a ramp rate of 60 °C/min under Ar flow with an average regulator output pressure of 50 kPa.

Results and discussion

We first investigated the effects of EWF on the conductivity of $Ti_3C_2T_x$ MXene films through altering the voltage by increments of 0.5 V followed by measurements of the subsequent resistance change of the MXene films. In this experiment, we measured electrical resistance of 2 mm long, 1 mm wide and ~ 2.2 µm thick $Ti_3C_2T_x$ sample at room temperature by passing electrical current on a probe station with Kelvin connection to eliminate contact resistance (Fig. 1a inset). Each data point has been taken three times and the variation of data is within 5% uncertainty. The rate of change is high initially and gradually flattens out to a fixed value. First, as shown in Fig. 1a, we noticed that low voltages (0.5–0.75 V and maximum current density 29.54 Amp/mm^2) using EWF did not alter the film resistivity significantly. At 1 V, we noticed a resistivity change of the MXene film from an original resistivity of 15.6 µΩ-m to 13.8 µΩ-m. By increasing the voltage beyond 1 V (current density 42.34 Amp/mm^2), the resistivity of the $Ti_3C_2T_x$ MXene film decreases significantly, with a minimum film resistivity of 4.3 µΩ-m when annealing with EWF at 3 V (current density 377.27 Amp/mm^2). At 2 V (current density 165.9 Amp/mm^2) resistivity decreased by 57% with only 15 °C temperature rise. The decrease of resistivity was ultra-fast as we observed the changes to be instantaneous. The decreases in EWF-annealed $Ti_3C_2T_x$ MXene films resistivities are similar

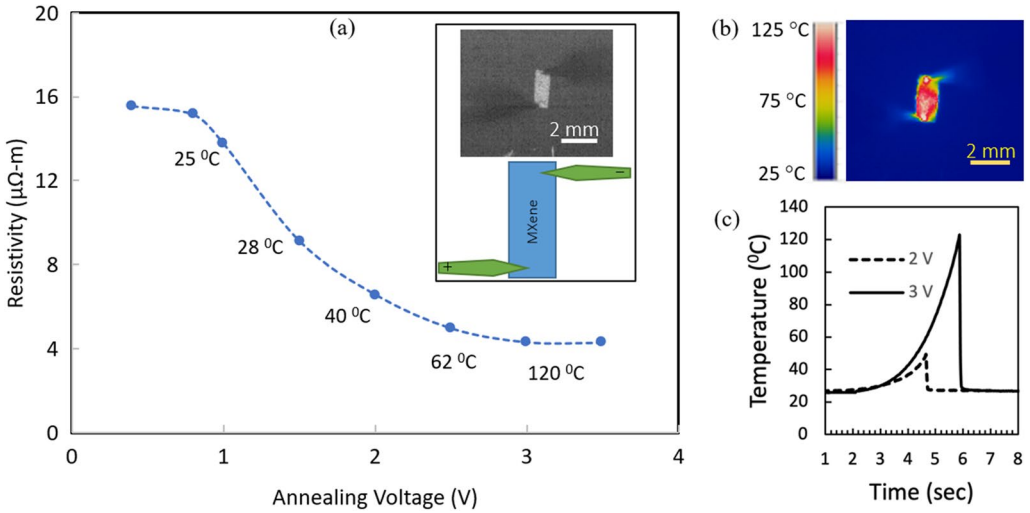

Figure 1: Effect of annealing voltage during EWF application on the resistivity of the $Ti_3C_2T_x$ MXene films and their temperature. (a) Voltage vs. resistivity curve. We sourced the voltage and measured the current to find resistance. Inset shows the digital photo (top) and schematic (bottom) of the measurement setup. (b) IR image of MXene at 3 V. (c) Time–temperature graph of the MXene film at 2 and 3 V.

to previous EWF studies, which showed improvement of crystallinity, reduction of defects and grain boundary density thus enhancement of electrical properties in metals and 2D materials [44–46]. Overall, we have seen up to a 72% decrease in resistivity at 3 V. In comparison, Hart et al. [34] reported about 64% decrease at 700 °C anneal inside high vacuum condition of the transmission electron microscope. However, beyond 3.5 V applied voltage we found no improvement in resistivity, which indicates that this process is sufficient to decrease resistivity of $Ti_3C_2T_x$ MXene films at an applied voltage of 3 V.

To minimize the temperature rise in the MXene films during EWF application, we used a large AlN slab as a heat sink. As shown in Fig. 1b and c, we tracked the temperature rise during the experiment with a thermal camera. With this method, we noted that the temperature rise is less than 50 °C for up to 2 V and up to 120 °C between 2 to 3 V. While our objective is to demonstrate the non-thermal nature of EWF annealing, it requires complete removal of the Joule heating associated with the process. Our approach of using a massive heatsink to eliminate Joule heating was therefore not completely effective, as reflected by this temperature rise. In future, this can be improved by enhancing forced convective heat transfer with blowing cold air on the specimen. As shown by Raman and XRD spectra, this temperature increase did not cause clear oxidation in the $Ti_3C_2T_x$ sample (Figs. 2 and 3). The decrease in resistant became less discernible beyond 3 V (current density 377.27 Amp/mm^2). Since the specimen is cooled only passively, temperature begins to rise rapidly. For example, at 3.5 V, the temperature reached about 275 °C without any further decrease in resistivity. This indicates that better results may be achieved with active cooling

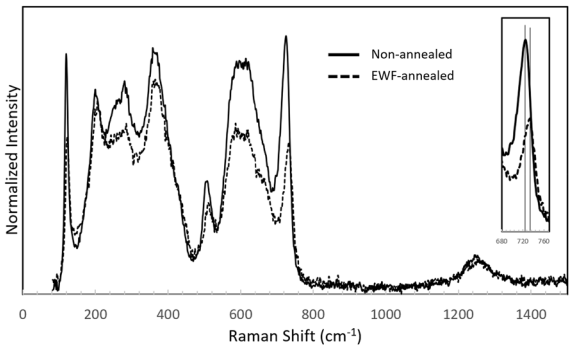

Figure 2: Effect of annealing on $Ti_3C_2T_x$ Raman peaks. The inset figure shows the most significant Raman shift that happens at 726.5 cm^{-1}.

and lower applied voltages. Lower temperature will also minimize the chances of oxidation.

In order to understand the effect of EWF on lowering the resistivity of the MXene specimens, we performed Raman spectroscopy and XRD methods before and after annealing. Raman spectroscopy characterizes the vibrational energy of the $Ti_3C_2T_x$ specimens and provides important information on chemical elements and their bonding. To identify any changes in the Raman spectrum, Lorentzian peak fitting was performed in the Origin software from 0 to 860 cm^{-1} Raman bands. Raman active vibrations in $Ti_3C_2T_x$ have been predicted theoretically [49]. Furthermore, these peaks have been assigned experimentally in multiple studies to investigate alteration in surface functional groups and intercalant [30]. A recent study on systematic change in Raman spectra of $Ti_3C_2T_x$ with synthesis-route-dependent variation in

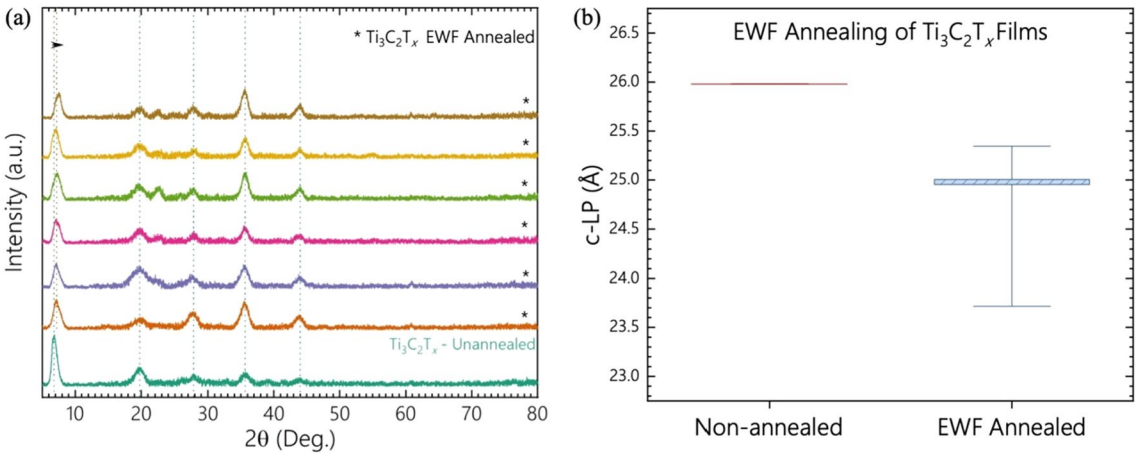

Figure 3: (a) XRD scans for the $Ti_3C_2T_x$ specimens before and after EWF annealing. Six samples were annealed via EWF. (b) *c*-lattice parameter (*c*-LP) derived from the (002) peak of the XRD patterns.

terminal groups sheds more light on controlling MXene behavior [48]. Raman spectroscopy was performed on EWF-annealed $Ti_3C_2T_x$ films as shown in Fig. 2, where the first peak appears at around 122 cm^{-1} for both annealed and post-annealed sample although the latter one has significantly less intensity. This is called the plasmon resonance peak, which occurs when the laser frequency (785 nm in this study) matches the plasmon oscillation. The next peak around 200 cm^{-1} is the out-of-plane vibration of C-Ti-T_x in MXene unit cell [48]. This peak does not show any significant change in intensity after EWF annealing of the MXene film.

The next peaks from 230 to 470 cm^{-1} comes from the in-plane vibration of surface atoms connected to titanium atoms. As this region is only affected by surface terminations, it can be used to understand any changes in the surface atoms. After annealing, we observed a reduction in Raman intensity from 210 to 470 cm^{-1} which indicates that the quantity of =O, –H and –F terminations have been reduced. Surface terminations are introduced during synthesis process of $Ti_3C_2T_x$ and its effects on conductivity ranges from conductive behavior to insulator [40, 50]. Previous studies have shown the removal of surface terminations at temperature above 200 °C to 700 °C [34–37]. However, while in our measurement temperature rise is moderate (up to 120 °C), we still observe a decrease in T_x content.

Figure 2 inset shows that the out-of-plane C vibration for non-annealed sample shifted from 726.5 to 732.5 cm^{-1} after annealing. This is the next most sharp peak other than the resonance peak, and its shifting to higher frequency number, which has been speculated to be due to two potential factors: decreased inter-flake distance of $Ti_3C_2T_x$ MXene layers or decreased defect concentrations in $Ti_3C_2T_x$ flakes [48]. As shown in Fig. 3, the *c*-lattice parameters (*c*-LP) derived via the (002) peak of $Ti_3C_2T_x$ films from their XRD patterns indicate an average decrease in inter-flake distances due to EWF annealing of approximately 0.5 Å. In addition, no clear TiO_2 oxide formation is visible in Fig. 3a. Therefore, we speculate that the shifting of the out-of-plane C resonance peak as seen in Raman spectra shown in Fig. 2 is due to a decreased concentration of intra-flake defects in $Ti_3C_2T_x$ layers. This migration of defects and partial removal of the surface terminations in $Ti_3C_2T_x$ can be speculated to be a source of the decrease in resistivity in our EWF-annealed $Ti_3C_2T_x$ films as compared to the control film. Raman analysis can be summarized to show clear evidence of partial de-functionalization of –OH, –F and –Cl chemical species by the EWF, which has not been studied or reported before. We did not observe appreciable de-intercalation of the water molecules, probably because the EWF process is inherently a low temperature one.

Our experimental approach decouples Joule heating from the EWF so that the observed improvement in electrical property can be attributed to solely to EWF at low voltage where the rate of change in resistivity is higher. We hypothesize that current density, far less than the critical value for electromigration [51], can improve the intra-layer properties of MXene by using EWF by targeting defects like intra-flake interfaces (analogous to grain boundaries in polycrystalline metals). Grain boundary growths and strong coupling between flakes because of more ordered orientation can contribute to the increased conductivity of MXene films after annealing by EWF, even without any evidence of intercalated water removal. EWF's processes energize only electrons and direct them toward defect sites to transfer their momentum. This contrasts with thermal annealing's tendency which imparts equal vibrational energy to both defects and the lattice and randomizes the diffusion of energy carriers. Figure 4 shows the cross-section scanning electron micrographs of the MXene specimens before and after the EWF processing.

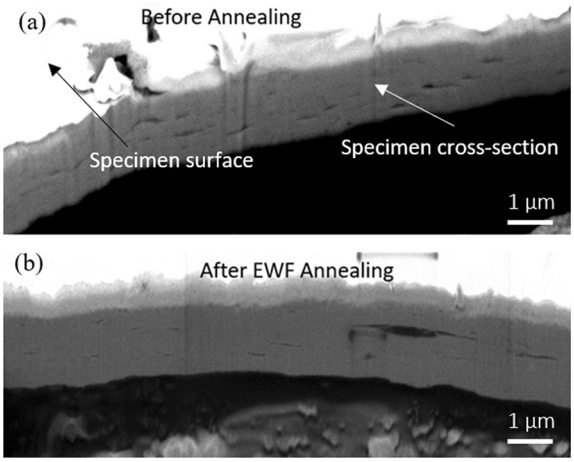

Figure 4: Cross-sectional SEM image of a $Ti_3C_2T_x$ film before (a) and after the EWF annealing (b).

The images show that the EWF magnitude is not large enough to heal cracks or voids of micron scales in the cross-section of the MXene films. While comparison of Fig. 4a with 4b can suggest a decrease in the frequency and volume of the micro voids, further characterizations are needed to determine whether this was due to the EWF power. Regardless, based on our XRD, it is clear that the inter-flake spacing is not affected at the level of the regular thermal annealing, where a ~ 2.5 Å reduction is observed in the $Ti_3C_2T_x$ MXene films due to the removal of the intercalated water molecules.

While the findings of this study indicate the effectiveness of the proposed EWF annealing, it is important to compare that with the conventional route of thermal annealing. As discussed earlier, it takes about 800 °C to remove both the intercalated water and surface groups [34]. We therefore performed thermal annealing at 800 °C in argon environment for one hour. The resistivity measured after thermal annealing is about 1.73 μΩ-m, which is lower than the 4.3 μΩ-m value achieved with EWF annealing. However, the EWF technique does not need any special environment and operates at significantly lower temperatures. As seen previously, phase transformation occurs at temperatures exceeding 700 °C in $Ti_3C_2T_x$, which results in mixed phases of $Ti_3C_2T_x$ MXene and cubic structures Ti_2C and TiC_y ($0.5 \le y \le 1$) [4]. To illustrate the effects of phase transformation on $Ti_3C_2T_x$, in situ X-ray diffraction techniques were used to analyze the crystal structure change of $Ti_3C_2T_x$ to Ti_2C and TiC_y. As seen in Fig. 5a, phase transformation of $Ti_3C_2T_x$ to Ti_2C and TiC_y occurs at roughly 700 °C, while near-complete phase transformation occurs at temperatures above 700 °C. Right-shifting of the (004), (006), and (008) peaks of $Ti_3C_2T_x$ up to 700 °C illustrate the *c*-LP shift to 20.02 Å, which is 5 Å less than that of EWF-annealed $Ti_3C_2T_x$. As compared to the control film, the electrical resistivity of these in situ annealed films increases from 0.56 μΩ m up to 2.50 μΩ m at 600 °C, which decreases to 1.43 μΩ m at 700 °C, as shown in Fig. 5b. This increase in electrical resistivity could be accounted to increased disorder during film annealing at 600 °C to partial phase transformation at 700 °C. This illustrates that high-temperature annealing processes to remove surface groups on bulk MXene films can potentially result in detrimental effects on the electrical conductivity of $Ti_3C_2T_x$ films due to escaping structural water as well as partial phase transformation [4]. The ex situ scan of $Ti_3C_2T_x$ film annealed at 800 °C for 1 h in a tube furnace is shown in Fig. 5c with a *c*-LP of $Ti_3C_2T_x$ of 19.76 Å with present Ti_2C and TiC_y phases [4].

To obtain insights on the structural and surface groups differences between the EWF and thermal annealing, we performed Raman spectroscopy analysis on a $Ti_3C_2T_x$ tube furnace annealed at 800 °C for 1 h. This is shown in Fig. 6, where interestingly, the plasmon peak at 122 cm^{-1} does not appear. In Fig. 2, we noticed that EWF also diminishes this peak, suggesting that the free electron gas density decreases with both techniques. The peaks from 230 to 470 cm^{-1} are slightly higher in thermal annealing, which suggests incomplete elimination of the surface groups, since these peaks reflect the out-of-plane

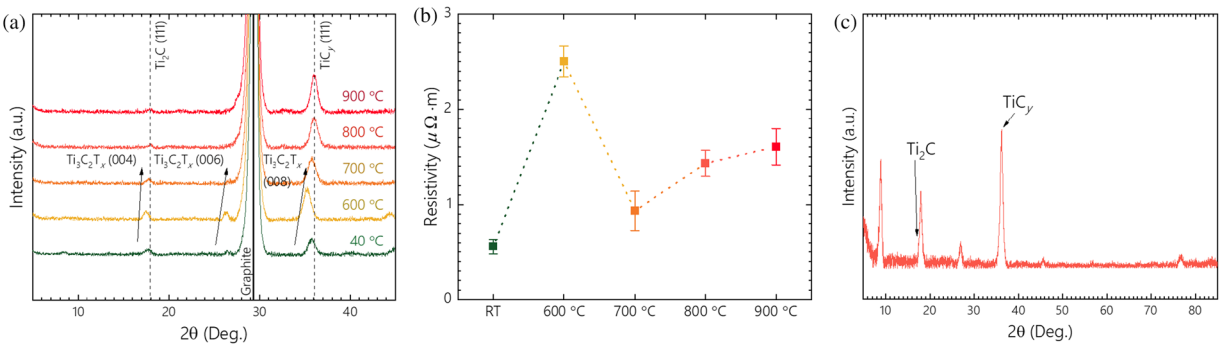

Figure 5: In situ XRD analysis of sequential annealing of $Ti_3C_2T_x$ films shown in (a) and the annealing effects on the electrical resistivity shown in (b). Data shown in (a) and (b) were reproduced from previous works [4]. Ex situ XRD scan of the $Ti_3C_2T_x$ tube furnace annealed at 800 °C for 1 h is shown in (c)

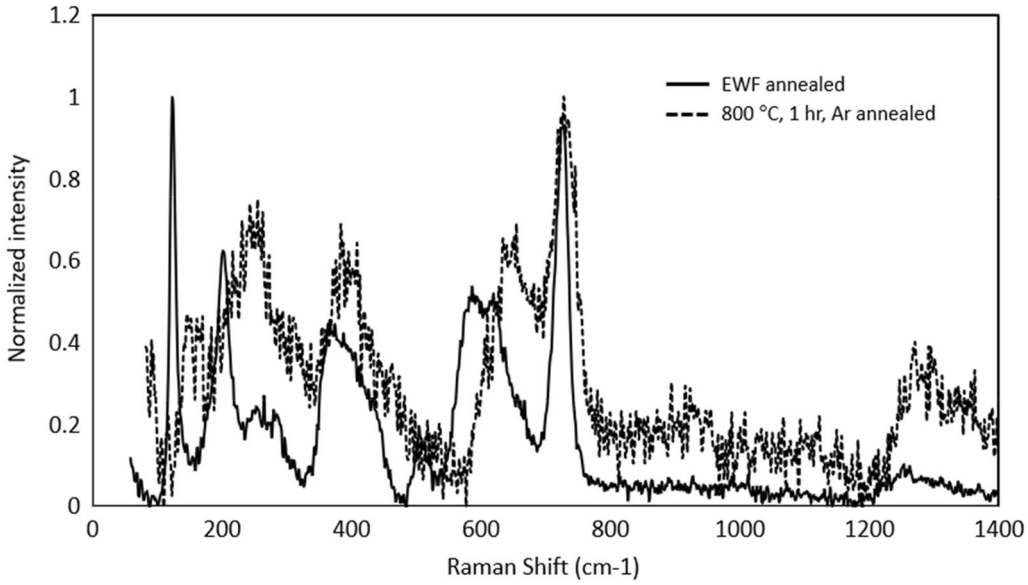

Figure 6: Comparison of EWF and thermal annealing effects on Raman spectra.

vibration of C-Ti-T_x. The region between 580 and 730 cm^{-1} mostly reflects carbon vibrations. Again, the thermally annealed specimens indicated increase in the peak, which could possibly be due to the appearance of disordered sp^3 carbon in the system (D-band peak around 1300 cm^{-1}), which is known to happen at higher temperatures, or due to the decreased interlayer distance between the flakes in the structure.

Comparison of the characteristic MXene peaks therefore suggest that the thermally annealed specimens do not exhibit significantly better removal of the surface terminal groups, but the low electrical resistivity may originate from the removal of the intercalated water. Since EWF annealing took place at around 120 °C, the water content most likely was only partially removed evident by our XRD results (Fig. 3). EWF's capability at removing surface groups without excess thermal annealing processes which may result in phase transformation of $Ti_3C_2T_x$ to Ti_2C and/or TiC_y phases indicates the potential of this process to be used as an ambient process to increase conductivity of $Ti_3C_2T_x$ films by migrating defects and removing surface groups off of the surface of $Ti_3C_2T_x$. However, further work will be necessary to extract the exact mechanism of EWF's improvement in resistivity as compared to that of thermal annealing.

In summary, we synthesized and measured the in-plane resistivity of $Ti_3C_2T_x$ before and after annealing with electrical stimulus. Electrical stimulus produces both EWF and joule heating due to electron–phonon and electron–defect interactions, respectively. By passively removing the Joule heat, we were able to promote the EWF effects. We show evidence of EWF-induced electrical resistivity decrease of about 57% and 72% at current densities of 165.9 and 377.27 Amp/mm^2, respectively. The corresponding specimen temperatures were only 40 and 120 °C, respectively. According to our hypothesis, the EWF improved the film quality by transferring energy to the defective regions only. Raman data provide evidence of reduction in the surface terminations. XRD show a small change in the lattice parameter (0.5 Å) indicating that the reduction in the MXene film resistivity is not due to the large inter-flake distance changes (~ 5 Å) usually observed in the thermal annealing of the MXene films. The underlying mechanisms are suggested to be surface termination de-functionalization and inter-flake defects removal. Our findings may offer valuable insight of improving material quality by applying energy and time-efficient approach.

Acknowledgments

MAH gratefully acknowledges the support from the Division of Civil, Mechanical, & Manufacturing Innovation (Nanomanufacturing program) of the National Science Foundation through award # 1760931. BA acknowledges the support from Indiana University Research Support Funds Grant (RSFG) and startup funding from the Department of Mechanical and Energy Engineering and Purdue School of Engineering and Technology at IUPUI. We would like to also acknowledge the use of Bruker XRD equipment, which was awarded through NSF grant MRI-1429241. The help of Ms. Krista Pulley with $Ti_3C_2T_x$ synthesis is greatly appreciated.

Availability of data and material

Data and material for this manuscript will be available upon request.

Declarations

Conflict of interest We declare no conflict or competing interests.

References

1. C. Shi, M. Beidaghi, M. Naguib, O. Mashtalir, Y. Gogotsi, S.J. Billinge, Structure of nanocrystalline Ti_3C_2 MXene using atomic pair distribution function. Phys. Rev. Lett **112**(12), 125501 (2014)
2. M. Naguib, O. Mashtalir, J. Carle, V. Presser, J. Lu, L. Hultman, Y. Gogotsi, M.W. Barsoum, Two-dimensional transition metal carbides. ACS Nano **6**(2), 1322–1331 (2012)
3. T. Mathis, M. Maleski, A. Goad, A. Sarycheva, M. Anayee, A. C. Foucher, K. Hantanasirisakul, E. Stach, Y. Gogotsi, Modified MAX phase synthesis for environmentally stable and highly conductive Ti_3C_2 MXene. ChemRxiv (2020)
4. B.C. Wyatt, S.K. Nemani, K. Desai, H. Kaur, B. Zhang, B. Anasori, High-temperature stability and phase transformations of Titanium Carbide ($Ti_3C_2T_x$) MXene. J. Phys.: Condens. Matter **33**(22), 224002 (2021)
5. C.E. Shuck, A. Sarycheva, M. Anayee, A. Levitt, Y. Zhu, S. Uzun, V. Balitskiy, V. Zahorodna, O. Gogotsi, Y. Gogotsi, Scalable synthesis of $Ti_3C_2T_x$ MXene. Adv. Eng. Mater. **22**(3), 1901241 (2020)
6. J. Zhang, N. Kong, S. Uzun, A. Levitt, S. Seyedin, P.A. Lynch, S. Qin, M. Han, W. Yang, J. Liu, Scalable manufacturing of free-standing, strong $Ti_3C_2T_x$ MXene films with outstanding conductivity. Adv. Mater. **32**(23), 2001093 (2020)
7. B. Anasori, Y. Xie, M. Beidaghi, J. Lu, B.C. Hosler, L. Hultman, P.R. Kent, Y. Gogotsi, M.W. Barsoum, Two-dimensional, ordered, double transition metals carbides (MXenes). ACS Nano **9**(10), 9507–9516 (2015)
8. M. Khazaei, M. Arai, T. Sasaki, M. Estili, Y. Sakka, Two-dimensional molybdenum carbides: potential thermoelectric materials of the MXene family. Phys. Chem. Chem. Phys. **16**(17), 7841–7849 (2014)
9. W. Hong, B.C. Wyatt, S.K. Nemani, B. Anasori, Double transition-metal MXenes: atomistic design of two-dimensional carbides and nitrides. MRS Bull. **45**(10), 850–861 (2020)
10. M. Dahlqvist, J. Lu, R. Meshkian, Q. Tao, L. Hultman, J. Rosen, Prediction and synthesis of a family of atomic laminate phases with Kagomé-like and in-plane chemical ordering. Sci. Adv. **3**(7), e1700642 (2017)
11. V. Kamysbayev, A.S. Filatov, H. Hu, X. Rui, F. Lagunas, D. Wang, R.F. Klie, D.V. Talapin, Covalent surface modifications and superconductivity of two-dimensional metal carbide MXenes. Science **369**(6506), 979–983 (2020)
12. Y. Liu, H. Xiao, W.A. Goddard III., Schottky-barrier-free contacts with two-dimensional semiconductors by surface-engineered MXenes. J. Am. Chem. Soc. **138**(49), 15853–15856 (2016)
13. M. Khazaei, M. Arai, T. Sasaki, C.Y. Chung, N.S. Venkataramanan, M. Estili, Y. Sakka, Y. Kawazoe, Novel electronic and magnetic properties of two-dimensional transition metal carbides and nitrides. Adv. Func. Mater. **23**(17), 2185–2192 (2013)
14. M.Q. Zhao, C.E. Ren, Z. Ling, M.R. Lukatskaya, C. Zhang, K.L. Van Aken, M.W. Barsoum, Y. Gogotsi, Flexible MXene/carbon nanotube composite paper with high volumetric capacitance. Adv. Mater. **27**(2), 339–345 (2015)
15. M. Naguib, J. Come, B. Dyatkin, V. Presser, P.-L. Taberna, P. Simon, M.W. Barsoum, Y. Gogotsi, MXene: a promising transition metal carbide anode for lithium-ion batteries. Electrochem. Commun. **16**(1), 61–64 (2012)
16. Y. Xie, Y. Dall'Agnese, M. Naguib, Y. Gogotsi, M.W. Barsoum, H.L. Zhuang, P.R. Kent, Prediction and characterization of MXene nanosheet anodes for non-lithium-ion batteries. ACS Nano **8**(9), 9606–9615 (2014)
17. M.R. Lukatskaya, O. Mashtalir, C.E. Ren, Y. Dall'Agnese, P. Rozier, P.L. Taberna, M. Naguib, P. Simon, M.W. Barsoum, Y. Gogotsi, Cation intercalation and high volumetric capacitance of two-dimensional titanium carbide. Science **341**(6153), 1502–1505 (2013)
18. Y. Dall'Agnese, M.R. Lukatskaya, K.M. Cook, P.-L. Taberna, Y. Gogotsi, P. Simon, High capacitance of surface-modified 2D titanium carbide in acidic electrolyte. Electrochem. Commun. **48**, 118–122 (2014)
19. B. Anasori, M.R. Lukatskaya, Y. Gogotsi, 2D metal carbides and nitrides (MXenes) for energy storage. Nat. Rev. Mater. **2**(2), 1–17 (2017)
20. M. Ghidiu, M.R. Lukatskaya, M.-Q. Zhao, Y. Gogotsi, M.W. Barsoum, Conductive two-dimensional titanium carbide 'clay'with high volumetric capacitance. Nature **516**(7529), 78–81 (2014)
21. M. Han, X. Yin, H. Wu, Z. Hou, C. Song, X. Li, L. Zhang, L. Cheng, Ti_3C_2 MXenes with modified surface for high-performance electromagnetic absorption and shielding in the X-band. ACS Appl. Mater. Interfaces **8**(32), 21011–21019 (2016)
22. M. Han, C.E. Shuck, R. Rakhmanov, D. Parchment, B. Anasori, C.M. Koo, G. Friedman, Y. Gogotsi, Beyond $Ti_3C_2T_x$: MXenes for electromagnetic interference shielding. ACS Nano **14**(4), 5008–5016 (2020)
23. Q. Peng, J. Guo, Q. Zhang, J. Xiang, B. Liu, A. Zhou, R. Liu, Y. Tian, Unique lead adsorption behavior of activated hydroxyl group in two-dimensional titanium carbide. J. Am. Chem. Soc. **136**(11), 4113–4116 (2014)
24. Y. Ying, Y. Liu, X. Wang, Y. Mao, W. Cao, P. Hu, X. Peng, Two-dimensional titanium carbide for efficiently reductive removal

of highly toxic chromium (VI) from water. ACS Appl. Mater. Interfaces **7**(3), 1795–1803 (2015)

25. M. Sokol, V. Natu, S. Kota, M.W. Barsoum, On the chemical diversity of the MAX phases. Trends Chem. **1**(2), 210–223 (2019)
26. M. Naguib, M. Kurtoglu, V. Presser, J. Lu, J. Niu, M. Heon, L. Hultman, Y. Gogotsi, M.W. Barsoum, Two-dimensional nanocrystals produced by exfoliation of Ti_3AlC_2. Adv. Mater. **23**(37), 4248–4253 (2011)
27. M. Alhabeb, K. Maleski, B. Anasori, P. Lelyukh, L. Clark, S. Sin, Y. Gogotsi, Guidelines for synthesis and processing of two-dimensional titanium carbide ($Ti_3C_2T_x$ MXene). Chem. Mater. **29**(18), 7633–7644 (2017)
28. Y. Li, H. Shao, Z. Lin, J. Lu, L. Liu, B. Duployer, P.O. Persson, P. Eklund, L. Hultman, M. Li, A general Lewis acidic etching route for preparing MXenes with enhanced electrochemical performance in non-aqueous electrolyte. Nat. Mater. **19**(8), 894–899 (2020)
29. M.A. Hope, A.C. Forse, K.J. Griffith, M.R. Lukatskaya, M. Ghidiu, Y. Gogotsi, C.P. Grey, NMR reveals the surface functionalisation of Ti_3C_2 MXene. Phys. Chem. Chem. Phys. **18**(7), 5099–5102 (2016)
30. M. Hu, T. Hu, Z. Li, Y. Yang, R. Cheng, J. Yang, C. Cui, X. Wang, Surface functional groups and interlayer water determine the electrochemical capacitance of $Ti_3C_2T_x$ MXene. ACS Nano **12**(4), 3578–3586 (2018)
31. Q. Tang, Z. Zhou, P. Shen, Are MXenes promising anode materials for Li ion batteries? Computational studies on electronic properties and Li storage capability of Ti_3C_2 and $Ti_3C_2X_2$ (X= F, OH) monolayer. J. Am. Chem. Soc. **134**(40), 16909–16916 (2012)
32. Y. Gogotsi, B. Anasori, *The Rise of MXenes* (ACS Publications, Washington, DC, 2019)
33. B.C. Wyatt, A. Rosenkranz, B. Anasori, 2D MXenes: tunable mechanical and tribological properties. Adv. Mater. **33**(17), 2007973 (2021)
34. J.L. Hart, K. Hantanasirisakul, A.C. Lang, B. Anasori, D. Pinto, Y. Pivak, J.T. van Omme, S.J. May, Y. Gogotsi, M.L. Taheri, Control of MXenes' electronic properties through termination and intercalation. Nat. Commun. **10**(1), 1–10 (2019)
35. Z. Zhang, Z. Yao, X. Zhang, Z. Jiang, 2D Carbide MXene under postetch low-temperature annealing for high–performance supercapacitor electrode. Electrochim. Acta **359**, 136960 (2020)
36. O. Kaipoldayev, Y. Mukhametkarimov, R. Nemkaeva, G. Baigarinova, M. Aitzhanov, A. Muradov, N. Guseinov, Studying of 2D titanium carbide structure by Raman spectroscopy after heat treatment in argon and hydrogen atmospheres. Eurasian Chem. Technol. J. **19**(2), 197–200 (2017)
37. H. Wang, Y. Wu, J. Zhang, G. Li, H. Huang, X. Zhang, Q. Jiang, Enhancement of the electrical properties of MXene Ti_3C_2 nanosheets by post-treatments of alkalization and calcination. Mater. Lett. **160**, 537–540 (2015)
38. C.J. Zhang, S. Pinilla, N. McEvoy, C.P. Cullen, B. Anasori, E. Long, S.-H. Park, A.S. Seral-Ascaso, A. Shmeliov, D. Krishnan, Oxidation stability of colloidal two-dimensional titanium carbides (MXenes). Chem. Mater. **29**(11), 4848–4856 (2017)
39. S. Huang, V.N. Mochalin, Hydrolysis of 2D transition-metal carbides (MXenes) in colloidal solutions. Inorg. Chem. **58**(3), 1958–1966 (2019)
40. B. Anasori, C. Shi, E.J. Moon, Y. Xie, C.A. Voigt, P.R. Kent, S.J. May, S.J. Billinge, M.W. Barsoum, Y. Gogotsi, Control of electronic properties of 2D carbides (MXenes) by manipulating their transition metal layers. Nanoscale Horiz. **1**(3), 227–234 (2016)
41. K.D. Fredrickson, B. Anasori, Z.W. Seh, Y. Gogotsi, A. Vojvodic, Effects of applied potential and water intercalation on the surface chemistry of Ti_2C and Mo_2C MXenes. J. Phys. Chem. C **120**(50), 28432–28440 (2016)
42. Z. Hemmat, P. Yasaei, J.F. Schultz, L. Hong, L. Majidi, A. Behranginia, L. Verger, N. Jiang, M.W. Barsoum, R.F. Klie, Tuning thermal transport through atomically thin $Ti_3C_2T_z$ MXene by current annealing in vacuum. Adv. Funct. Mater. **29**(19), 1805693 (2019)
43. Y. Lee, S.J. Kim, Y.-J. Kim, Y. Lim, Y. Chae, B.-J. Lee, Y.-T. Kim, H. Han, Y. Gogotsi, C.W. Ahn, Oxidation-resistant titanium carbide MXene films. J. Mater. Chem. A **8**(2), 573–581 (2020)
44. D. Waryoba, Z. Islam, B. Wang, A. Haque, Low temperature annealing of metals with electrical wind force effects. J. Mater. Sci. Technol. **35**(4), 465–472 (2019)
45. Z. Islam, A. Kozhakhmetov, J. Robinson, A. Haque, Enhancement of WSe_2 FET performance using low-temperature annealing. J. Electron. Mater. **49**(6), 3770–3779 (2020)
46. Z. Islam, H. Gao, A. Haque, Synergy of elastic strain energy and electron wind force on thin film grain growth at room temperature. Mater. Charact. **152**, 85–93 (2019)
47. M. Seredych, C.E. Shuck, D. Pinto, M. Alhabeb, E. Precetti, G. Deysher, B. Anasori, N. Kurra, Y. Gogotsi, High-temperature behavior and surface chemistry of carbide mxenes studied by thermal analysis. Chem. Mater. **31**(9), 3324–3332 (2019)
48. A. Sarycheva, Y. Gogotsi, Raman spectroscopy analysis of the structure and surface chemistry of $Ti_3C_2T_x$ MXene. Chem. Mater. **32**(8), 3480–3488 (2020)
49. T. Hu, J. Wang, H. Zhang, Z. Li, M. Hu, X. Wang, Vibrational properties of Ti_3C_2 and $Ti_3C_2T_2$ (T= O, F, OH) monosheets by first-principles calculations: a comparative study. Phys. Chem. Chem. Phys. **17**(15), 9997–10003 (2015)
50. L. Dong, H. Kumar, B. Anasori, Y. Gogotsi, V.B. Shenoy, Rational design of two-dimensional metallic and semiconducting spintronic materials based on ordered double-transition-metal MXenes. J. Phys. Chem. Lett. **8**(2), 422–428 (2017)
51. J. Lienig, M. Thiele, *Fundamentals of Electromigration-Aware Integrated Circuit Design* (Springer, Berlin, 2018)